Hindawi
Shock and Vibration
Volume 2018, Article ID 9753793, 13 pages
https://doi.org/10.1155/2018/9753793

Research Article

Development of Pyroshock Simulator for Shock Propagation Test

So-Jeong Lee, Dae-Hyun Hwang, and Jae-Hung Han

Department of Aerospace Engineering, KAIST, Daejeon 34141, Republic of Korea

Correspondence should be addressed to Jae-Hung Han; jaehunghan@kaist.ac.kr

Received 13 April 2018; Accepted 30 July 2018; Published 13 September 2018

Academic Editor: Franck Poisson

Satellites are subjected to pyrotechnic shocks caused by actuating the pyrotechnic separation devices during various missions such as separation from the launch vehicle and deployment of the solar panel. Pyroshock rarely damages structural members, but it may cause damage to mounted electronic equipment, which can lead to mission failures. In order to protect electronic equipment from pyroshock, shock propagation characteristics need to be identified. This paper proposes a compact pyroshock simulator that can be used to identify the pyroshock propagation characteristics at various locations of a structure. A small resonant fixture and high air pressure are used to make the simulator compact in size. A diaphragm breech design is also introduced to achieve high-bursting pressure and increase the repeatability of the simulator. The developed simulator can produce the pyroshock environment with repeatability in the shock propagation path, and also the pyroshock environment can be changed by using different resonant fixtures. The developed simulator can be used for the experimental characterization of the pyroshock propagation over various structures.

1. Introduction

Pyrotechnic separation devices have been widely used for the separation events of space systems because of their advantages in high energy per unit volume and high reliability, among others. The actuation of the pyrotechnic devices generates a localized, large pyroshock on the surrounding structures. Pyroshock rarely damages structures, but the high-frequency components of the shock motions propagating to the structure can cause malfunction or failure of mounted electronic equipment such as relay chatter, circuit shortage due to the breakage of lead wires, and dislodging of contaminants [1, 2]. In order to prevent those problems, a shock isolator is often used for each electronic equipment [3]. Although the isolators are effective for shock attenuation, the isolators need to be designed with trade-offs between the low-frequency vibration amplification and the pyroshock attenuation; the shock attenuation design of the structures is needed to reduce the pyroshock from the shock source to the electronic devices. Therefore, the pyroshock propagation test over various structures (the effects of structural interfaces, shock reduction for a certain type of structure) needs to be conducted. The requirement related to the pyroshock test facility is to simulate a propagation of a stress wave and to replicate the shock propagation path repeatedly.

Most pyroshock testing of qualifying sensitive equipment involves shock testing using pyrotechnic or non-pyrotechnic devices. Testing using pyrotechnic devices can simulate the near-field environment, but they have safety problems and require trial and error for repeatability [4–11]. Dilhan et al. [12] developed a pyroshock generator using an explosive device, and the purpose of the device is to cover a large range of equipment requirements. This device was designed in a relatively compact form using gunpowder, but there was an associated safety problem. As an alternative, the pyroshock simulators without pyrotechnic devices have been studied. To simulate the pyroshock, an electronic shaker and a pyroshock simulator that uses mechanical impact have been often used. Use of an electronic shaker guarantees a high repeatability, but there is a limitation in reaching the pyroshock level. The electronic shaker cannot simulate the pyroshock that is higher than 3,000 Hz, and the maximum acceleration of the shaker is normally limited to about 300 G [13]. For the mechanical impact, a resonant fixture is generally used to simulate the specific shock environment for the electronic equipment [14–20]. The resonant fixture is excited into resonance by a mechanical impact from a projectile, an impact hammer, or other impact devices (Figure 1). Davie and Bateman [14] studied pyroshock simulation using a tunable resonant fixture.

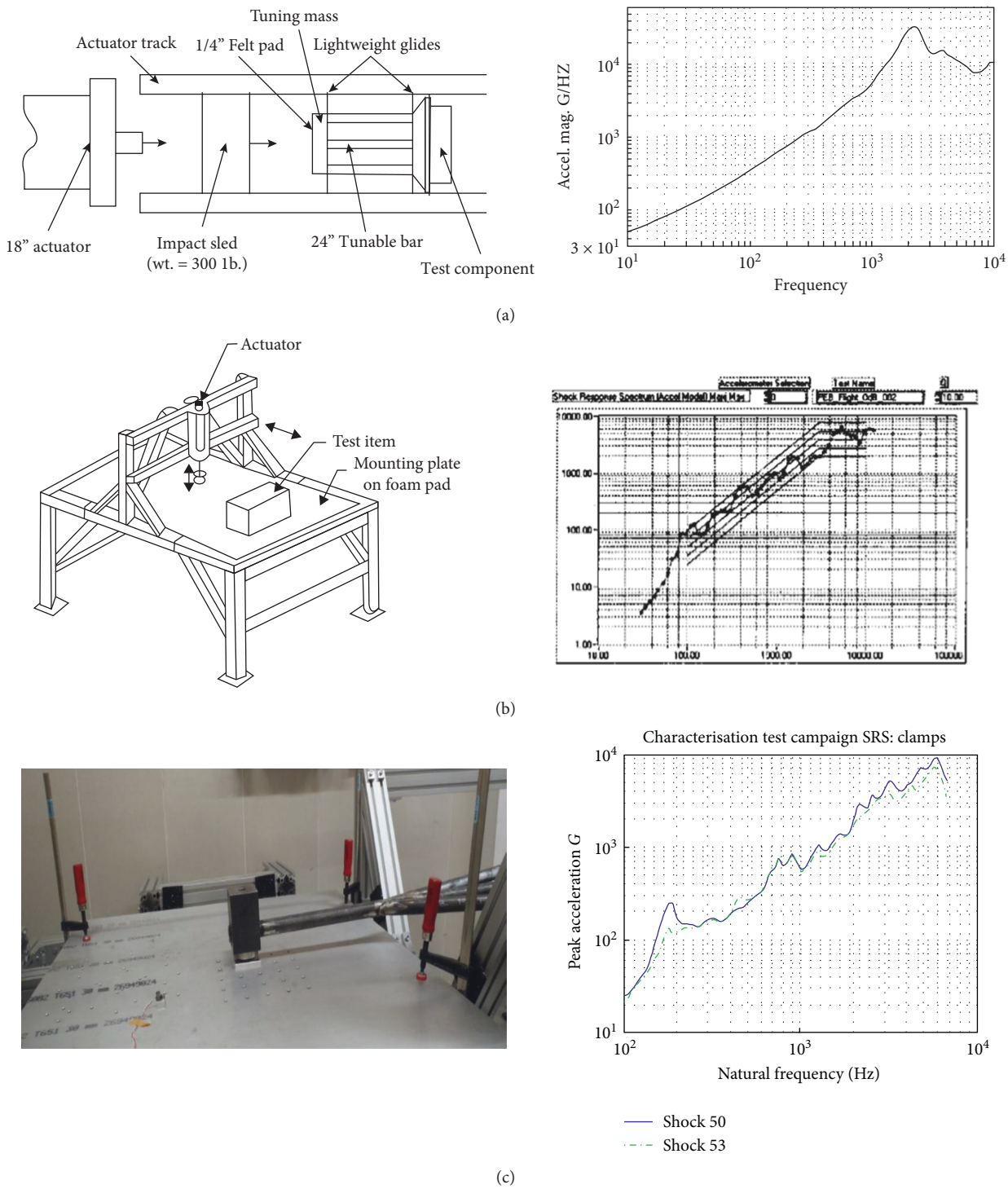

FIGURE 1: (a) Tunable resonant bar setup and SRS [14], (b) mechanical impulse pyroshock simulator (using resonant plate) and SRS [16], and (c) resonant plate with clamps and SRS [20].

The equipment attached at the end of the resonant bar is excited into longitudinal resonance (Figure 1(a)). Newell and James [16] developed a pneumatic actuated pyroshock simulator whose resonant plate is excited into resonance (Figure 1(b)). Jonsson [20] developed a pyroshock test facility for qualification of equipment. The resonant plate is excited into resonance with pendulum hammer (Figure 1(c)). Although these facilities can provide a required pyroshock environment by adjusting a test parameter, it is not affordable for pyroshock propagation test. Bateman and Brown [21] developed a pyroshock simulator that could simulate a propagation of a stress wave on the payload by actuating the V-band joint. However, due to the shape and size of the resonant fixture, only a circular impact environment could

be simulated and the shape and size of the test object structures were limited. Jeong et al. [22] developed a pyroshock simulation system to study the source isolation approach. This system could simulate a point shock source and the propagation of the stress wave by connecting the beam resonant fixture to the excitation location. The system was difficult to apply to various positions due to the shape and volume of the resonant fixture. Also, the repeatability for the shock propagation path has not been evaluated.

To study the characteristics of shock propagation over space structures, the simulator must be used at various positions of the structure and must have repeatability at a shock path to a measurement location from a shock source. In order to design a compact simulator without using pyrotechnic devices, a high-pressure air release device and a cylindrical resonant fixture are used. For the high-pressure air release device, a new method is applied by improving the double diaphragm breech method [23]. The shape of the resonant fixture is designed to generate a point source on a mounting structure. A bursting shape and a bursting pressure of a diaphragm are the most important factors of repeatability for the simulator. The bursting shape of the diaphragm is analyzed using ANSYS AUTODYN. As a result, the circular diaphragm with a Y-shape indentation on the center of the diaphragm is applied to the developed simulator. The repeatability of the simulator is evaluated based on the test tolerance introduced in the NASA standards [6]. The influence of the resonant fixture with different natural frequencies is also identified.

2. Design Procedure of the Simulator

2.1. Conceptual Design. The high-frequency excitation in a short duration, which is typical characteristics of a pyroshock, can be simulated by the sudden release of energy, such as a projectile's impact on the structure [13]. In this paper, a high-pressure release device is used to accelerate the light projectile rapidly.

The wrap-around breech method [24] and the double diaphragm breech method [23] are widely used as air release mechanisms. The breech mechanism is designed to block the air pressure and to release the air instantaneously at the desired pressure. However, the wrap-around method has limitations on the mass of a projectile and the volume of a barrel. This is because it requires sufficient strength of the projectile and the barrel. On the other hand, the double diaphragm method is not limited to the design of the barrel and the projectile, although the diaphragm is disposable and requires the use of multiple valves. To use the lightweight projectile, the double diaphragm method is more appropriate because there are no restrictions on a projectile and a barrel. To avoid the inconvenience of using multiple valves and a double diaphragm, one diaphragm and a solenoid valve are used to control the moment of the diaphragm bursting. The design concept of the device is shown in Figure 2. When the solenoid valve is operated, compressed air is released to burst the diaphragm instantaneously due to the pressure difference. The projectile behind the diaphragm is also accelerated. Figure 3 shows cross section and dimensions of the simulator which is the assembly of the chamber adapter, the chamber, the barrel, and the target. The solenoid valve is shown in Figure 4 and its specification is listed in Table 1. The projectile is made in a cylindrical shape with 8 mm of diameter and 5 mm of height, and it is made of stainless steel 630.

2.2. Release Device

2.2.1. Velocity Prediction of a Projectile. When the diaphragm bursts, the compressed air acting on the back of the diaphragm accelerates the projectile. The impact speed of the projectile is predicted by using a simple gas gun model, as shown in Figure 5 [25].

The motion equation of the projectile accelerated by the pressure of the chamber can be expressed as follows:

$$F = m\frac{d^2x}{dt^2} = mv\frac{dv}{dt} = AP(x) - AP_{\text{atm}} - f, \tag{1}$$

where m is the projectile mass, x and v are the distance of the projectile and velocity of the projectile, respectively, A and f are the area of the top of the projectile and friction force between the barrel and the projectile, P is the pressure of the chamber, and P_{atm} is the atmospheric pressure. Assuming that the expansion of the compressed air is a quasistatic isothermal process, as in the following equation:

$$P(x)(V_0 + Ax) = P_0V_0, \tag{2}$$

where V is the volume of the chamber and the subscript 0 means the initial value. The velocity of the projectile to the end of the barrel v_{end} is given by

$$v_{\text{end}} = \sqrt{\frac{2}{m}\left(P_0V_0\ln\left(1 + \frac{AL}{V_0}\right) - ALP_{\text{atm}} - Lf\right)}, \tag{3}$$

where L is the length of the barrel. The design variables are determined by iterative calculations. As a result of designing with the compressor specifications, a 3 g projectile can be launched at a speed of 82 m/s at a pressure of 50 bar. In order to adjust the bursting pressure, we controlled the thickness of the diaphragm.

2.2.2. Bursting Analysis of a Diaphragm. The major factor affecting the repeatability of the simulator is the bursting shape and bursting pressure of the diaphragm. The pressure applied to the projectile depends on the bursting shape of the diaphragm. The ANSYS software is used to expect the bursting pressure and the bursting shape of the diaphragm. The diaphragm is analyzed until it is burst by increasing pressure.

First, the geometry adjacent to the diaphragm is modeled to minimize the analysis time. The shape of the diaphragm is a circular plate with a diameter of 26 mm and thickness of 0.1 mm. As shown in Figure 6, a portion of the barrel is modeled at the bottom of the diaphragm and a portion of the chamber is modeled at the top.

After that, mesh modeling of the three parts is conducted. For accurate results and fast computational time,

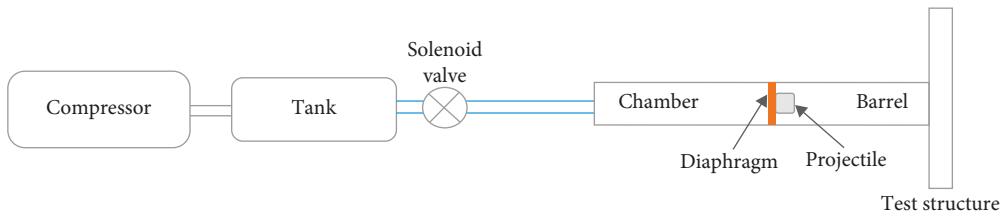

Figure 2: The conceptual design of the pyroshock simulator.

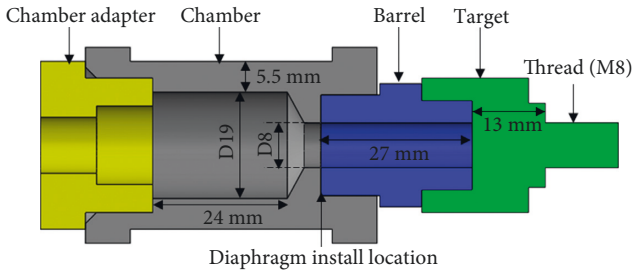

Figure 3: Cross section and dimensions of the simulator.

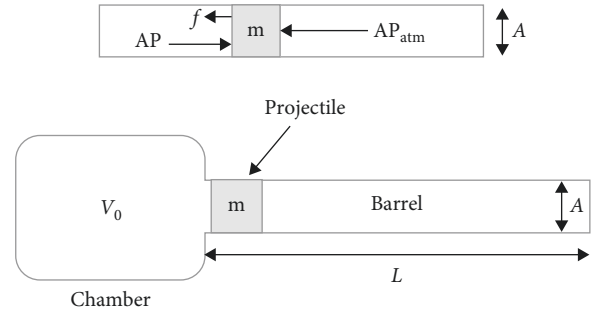

Figure 5: Schematic drawing of a simple one-stage gas gun.

Figure 4: The solenoid valve STH32C-15-4-T-H.

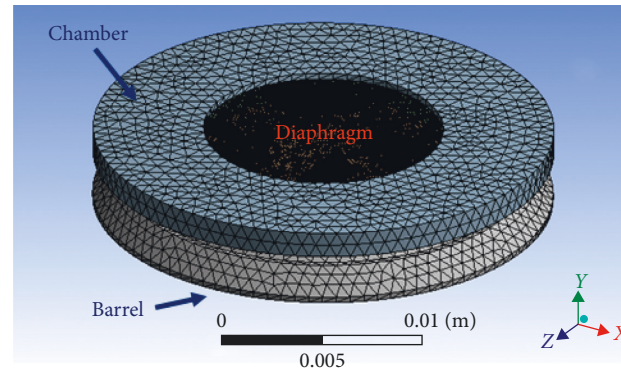

Figure 6: Geometric model and the meshing result of the diaphragm, the barrel, and the chamber.

Table 1: Specification of the solenoid valve.

Descriptions	Specification
Fluid	Air, water, oil, and steam
Operating	Normal closed
Port size	Rc(PT) 1/2 inch
Orifice size	14.5 mm
Response cycle	Max 80 ms

Table 2: Material properties of stainless steel 304.

Stainless steel 304		
Property	Value	Unit
Density	7,900	kg/m^3
Linear EOS		
Bulk modulus	166.7	GPa
Reference temperature	295	K
Bilinear strength		
Shear modulus	86	GPa
Yield stress	2.15	MPa
Tangent modulus	1.0	GPa
Failure model		
Plastic strain	0.7	

mesh modeling is important in ANSYS explicit because the time interval is determined by the Courant–Friedrichs–Lewy (CFL) condition [26]. Tetrahedral elements with a uniform size of 0.5 mm are used in the chamber and the barrel, and hexahedron elements with a uniform size of 0.1 mm are used in the diaphragm. The number of elements is 39,974 hexahedral elements and 28,500 tetrahedral elements.

The material of the diaphragm is modeled as stainless steel 304. The material properties define the density and linear state equations and failure theory to predict the

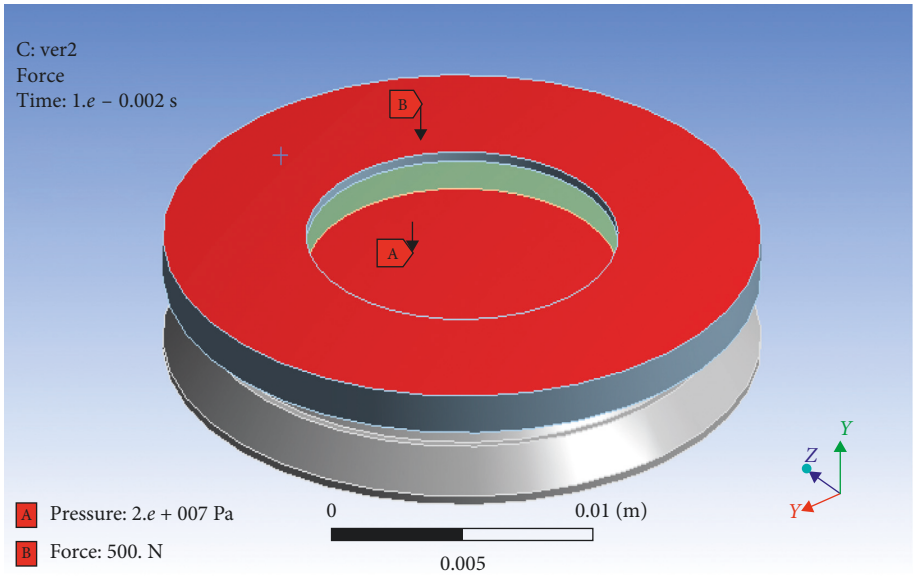

Figure 7: Boundary conditions on the analysis model.

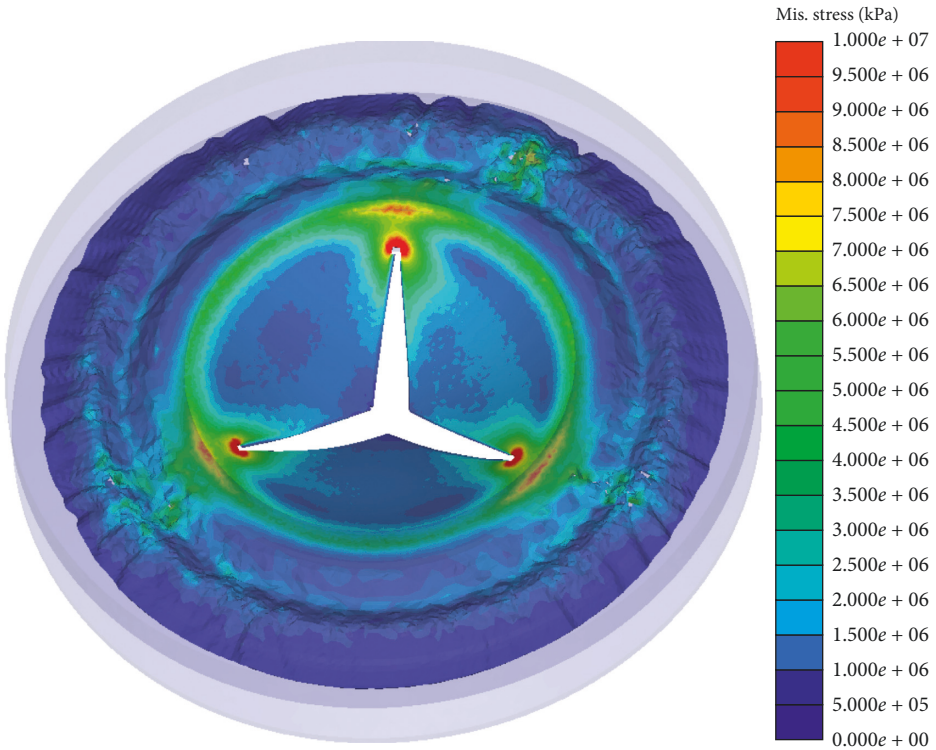

Figure 8: Bursting shape of the indented diaphragm.

bursting of the diaphragm. Plastic strain failure and bilinear strength model are used to simulate plastic and failure behavior. The plastic strain is defined as 0.7. The material properties of stainless steel 304 are summarized in Table 2.

A fixed boundary condition is applied to the bottom of the barrel, and a constant pressing load of 500 N is applied perpendicular to the upper part of the chamber to fix the diaphragm. The pressure boundary condition is defined as a ramp pressure of 200 bar during 10 ms at the upper surface of the diaphragm as shown in Figure 7.

An asymmetric bursting shape may result in a nonuniform pressure distribution to the projectile, and then, the simulator performance may be low. In order to prevent this phenomenon, a Y-shape indentation on the center of the diaphragm is considered so that the diaphragm bursts in the

center. The depth of the indentation is modeled as 0.03 mm. The analysis results reveal that the indented diaphragm bursts from the center, not from the edge of the diaphragm (Figure 8).

2.2.3. Resonant Fixture. The frequency at which the slope changes the shock response spectrum is called the knee frequency, which corresponds to the dominant frequency of the pyroshock environment [13]. The resonant fixture is designed so that the first mode natural frequency of the resonant fixture coincides with the knee frequency, and the dominant frequency is simulated by mechanical resonance. The resonant fixture is bolted between the target block and the test object structure.

To make the size of the simulator compact and generate a point-source shock on the test object structure, the shape of the resonant fixture is designed as a cylindrical shape with various numbers of design variables, as shown in Figure 9.

To understand the response of the resonant fixture, the device with a resonant fixture can be modeled as a three-degree-of-freedom (DOF) system, as shown in Figure 10. This model assumed that the assembly of the barrel and the chamber is rigid compared to the resonant fixture.

In Figure 10, M1 is the effective mass of the barrel and the chamber, M2 is the effective mass of the resonant fixture, and M3 is the effective mass of the bottom of the resonant fixture. k is the stiffness of the resonant fixture.

The main variables of the resonant fixture are the diameter (D) and thickness (t_1 and t_2) of the circular plate. To compare the effect of the resonator, two resonators are designed. The dimensions of two resonators and their natural frequencies are listed in Table 3. Figure 11 shows mode shapes of two resonators, which are obtained using ANSYS modal analysis.

In order to assume the barrel and the chamber as one lumped mass, it should have a natural frequency sufficiently higher than that of the resonator. Using ANSYS modal analysis, the axial natural frequency of the chamber-barrel assembly is found to be 21900 Hz (Figure 12); it is reasonable that the barrel and chamber are assumed to be one lumped mass.

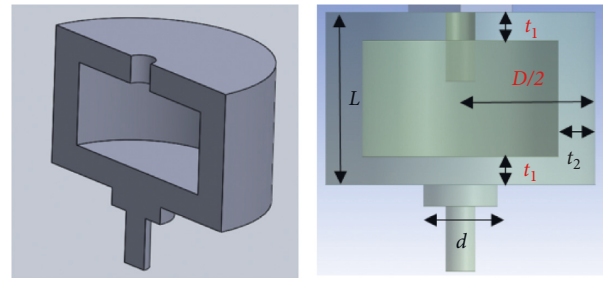

Figure 9: Shape and design parameters of the resonant fixture.

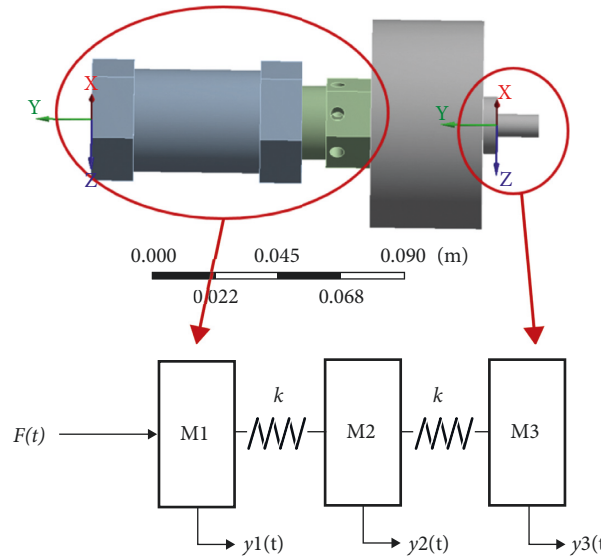

Figure 10: 3-DOF model for the assembly of the chamber, the barrel, and the resonator.

Table 3: Dimensions of the resonators.

Resonator type	Type 1	Type 2
Natural frequency (Hz)	6600	1100
L (mm)	40	40
D (mm)	73	110
d (mm)	20	20
t_1 (mm)	6.5	9.75
t_2 (mm)	3	8.8

3. Experiment

3.1. Experimental Setup. In order to evaluate the characteristic of the device, a pretest is performed. The test configuration is shown in Figure 13. The dimension of the test object structure is a 1000 mm × 500 mm × 5 mm plate made of aluminum alloy 6061, and the plate is clamped by a stainless steel fixture (Figure 14). The plate has four holes: one hole is for the simulator mounting and three threaded holes are for the shock accelerometer mounted to measure the shock signal. The shock is generated by the shock simulator. The material of the diaphragm is stainless steel 304, and the thickness is 0.1 mm.

The pyroshock is measured with an acceleration signal. The accelerometer can be saturated beyond the measurement range of the accelerometer sensor, and it may be damaged due to the accelerometer resonance when the accelerometer is located near the shock source. Therefore, an accelerometer with a built-in mechanical filter should be selected so that the sensor inside the accelerometer is not damaged [5, 6, 8, 25]. In order to obtain a valid signal without aliasing, a 1 MHz sampling rate is selected [27]. The specification of the acceleration and signal conditioner is listed in Table 4. The acceleration signal is measured at 30 mm, 150 mm, and 350 mm away from the shock source. The 10th-order Butterworth digital filter is applied to the measured acceleration signal in the range of 100 Hz to 10,000 Hz to eliminate

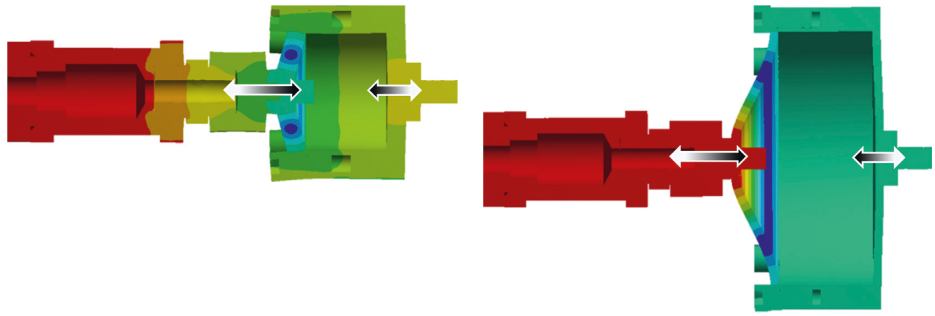

(a) (b)

Figure 11: Mode shape of the resonators in the axial direction: (a) type 1 and (b) type 2.

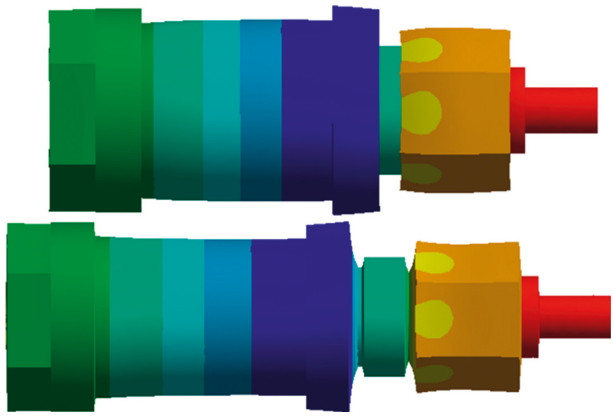

Figure 12: Mode shape of the chamber-barrel assembly in the axial direction (21900 Hz).

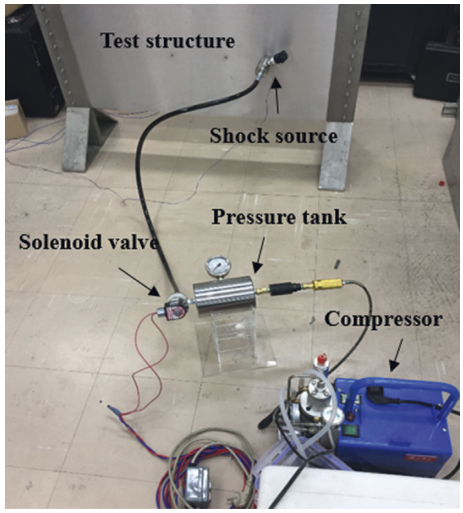

Figure 13: Configuration of the experiment setup.

high-frequency noise, aliasing, and low-frequency drift of the measured signal.

In the preliminary experiment, the projectile and the barrel made of aluminum alloy and stainless steel 304 are plastically deformed. The deformation of the barrel and projectile affects the impact duration so that the repeatability of the test results can be worse. Therefore,

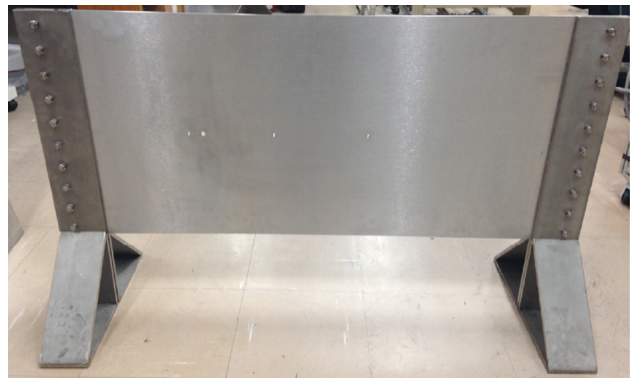

Figure 14: The clamped simple plate for pyroshock propagation experiment.

Table 4: Specifications of the accelerometer and signal conditioner.

Accelerometer (PCB 350B03)	
Sensitivity	0.5mV/G
Measurement range	±10,000 G peak
Frequency range (±1 dB)	0.4 to 10,000 Hz
Frequency range (−3 dB)	0.2 to 25,000 Hz
Mechanical filter resonant frequency	23,000 Hz
Resonant frequency	More than 100,000 Hz
Nonlinearity (per 10 kg)	Less than 2%
Transverse sensitivity	Less than 7%
Signal conditioner (NI PXI3-6366)	
Sample rate (single channel maximum)	2.00 MS/s
Number of channels	8, differential
ADC resolution	16 bits
Input coupling	DC
Input range	±10 V
Maximum working voltage for all analog inputs	±11 V
Bandwidth	1 MHz
Slew rate	20 V/μs

Table 5: Material properties of stainless steel 630 used in the projectile and the barrel.

	Stainless steel 630		
Condition	Density (kg/m^3)	Tensile strength (MPa)	Yield strength 0.2% proof (MPa)
H900 (projectile)	7750	1310	1170
H1150 (barrel)	7750	930	725

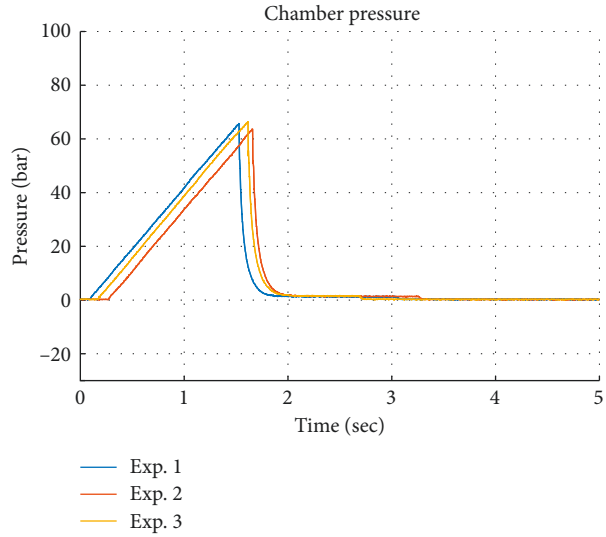

Figure 15: Pressure graph of the chamber.

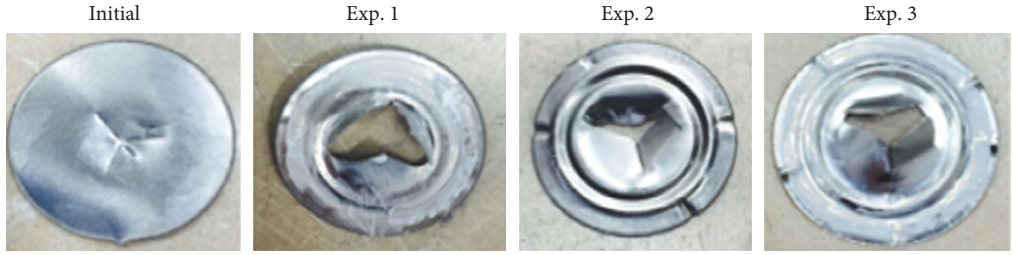

Figure 16: Bursting shape of the diaphragm. (a) Initial, (b) Exp. 1, (c) Exp. 2, (d) Exp. 3.

stainless steel 630, which has a higher yield strength than aluminum alloy and stainless steel 304, is selected. The material properties of stainless steel 630 are summarized in Table 5.

3.2. Repeatability Test. The experiments are carried out under the same conditions to evaluate the repeatability of the simulator in the pyroshock propagation path. The experiment is performed three times under the same conditions. The thickness of the diaphragm is 0.1 mm, and the resonant fixture is not used. The similarities of the measured acceleration time histories and calculated shock response spectrum (SRS) from the acceleration time histories are compared. The SRS is the most commonly used method to quantify pyroshock. The SRS means the maximum value of response for each natural frequency by applying shock excitation to the base of a system consisting of a single degree-of-freedom (SDOF) system with independent natural frequencies [28]. Although there is no standard for comparing SRS, the most commonly used criterion is the test tolerance provided by the NASA standards [6] or MIL standards [7]. In this study, the repeatability is evaluated using the test tolerance guided by the NASA standards. The tolerance most commonly used in practice is specified for the maximax SRS. The tolerance is ± 6 dB when the natural frequency is below 3,000 Hz and +9/−6 dB when the natural frequency is over 3,000 Hz.

If the test results are inside this criterion, they can be regarded as the same shock environment. In this study, the results are evaluated in the frequency range between 100 Hz and 10,000 Hz.

In the results of the experiment, the bursting pressure of the diaphragm is almost similar to the three experiments, as shown in Figure 15. The shape of the bursting diaphragm is similar as being torn into three branches (Y-shape) due to the indentation on the center of the diaphragm as well (Figure 16).

The acceleration time histories during 20 ms and acceleration SRS at 30 mm, 150 mm, and 350 mm points are shown in Figures 17 and 18, respectively. The comparison of the acceleration time histories shows a very similar initial response. According to the results of the SRSs of three experiments, when the distance increases, the difference of the results increases. They are within the tolerance criterion (the gray dotted line) at three positions. The results show that the simulator has a repeatability and can be properly used for the shock propagation test.

3.3. The Effect of the Resonant Fixture. The effect of the resonant fixture, which is designed to obtain the different

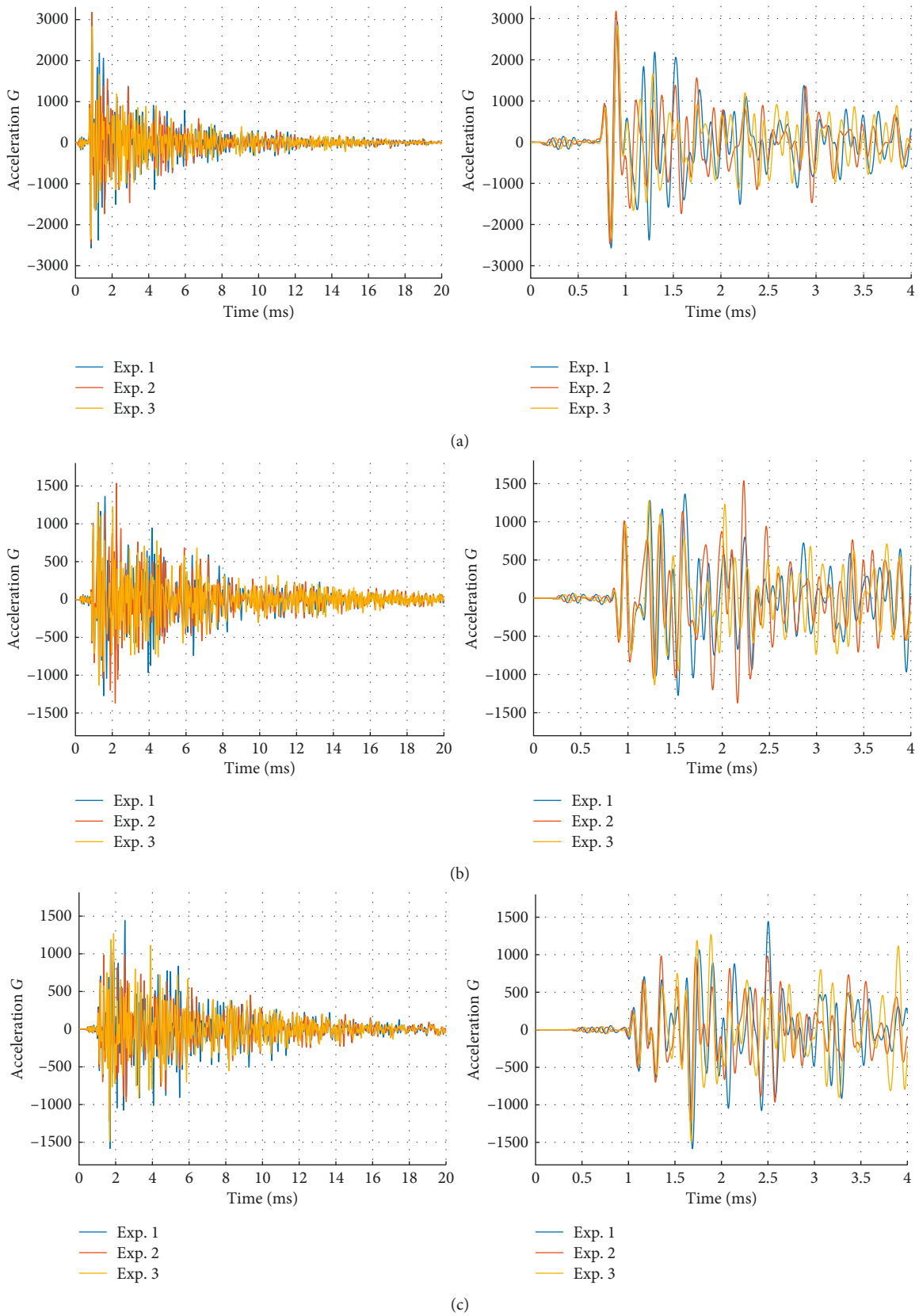

Figure 17: Acceleration time history (a) at 30 mm, (b) at 150 mm, and (c) at 350 mm from shock source.

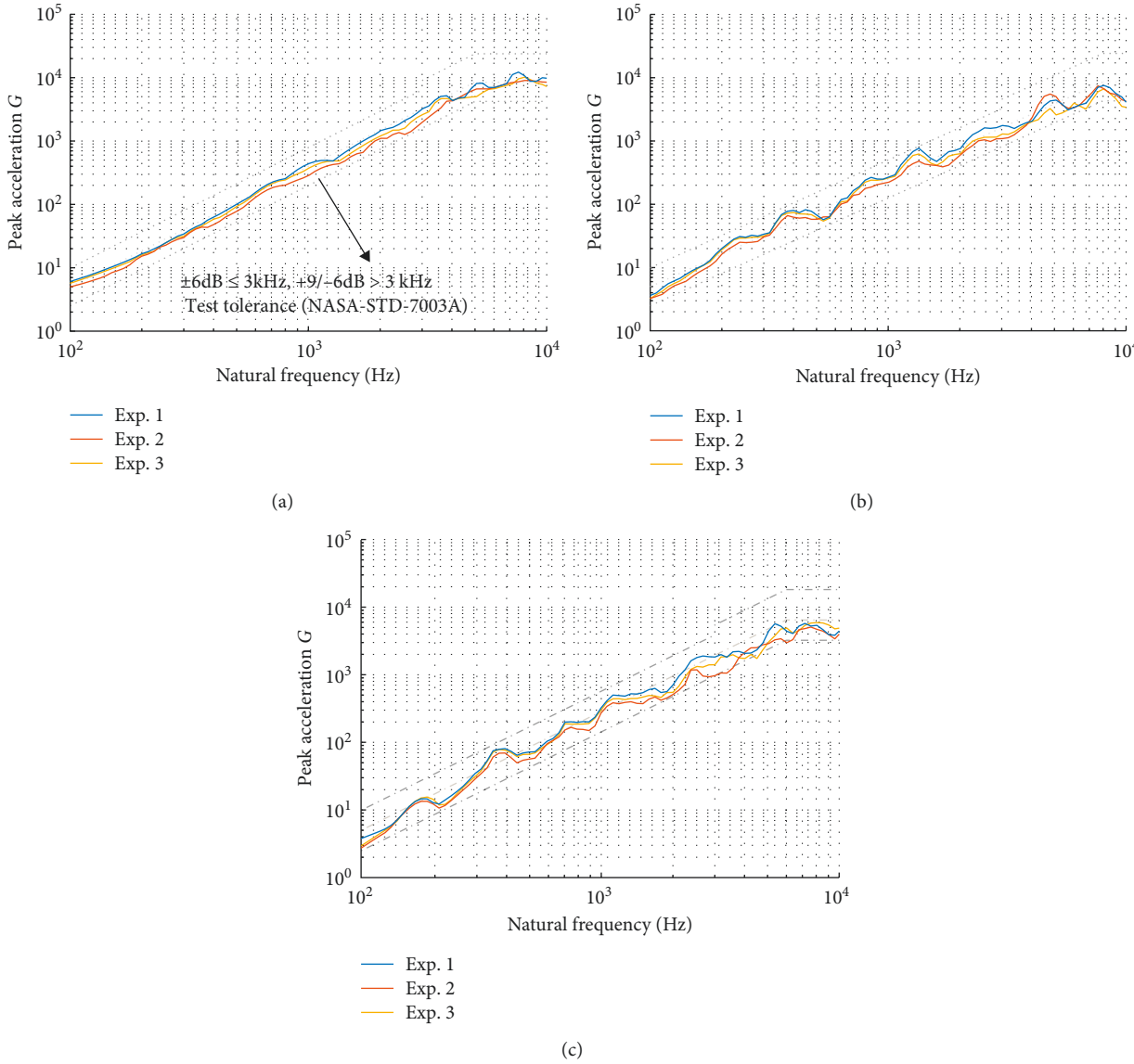

Figure 18: Acceleration SRS (a) at 30 mm, (b) at 150 mm, and (c) at 350 mm from shock source.

shock environment, is evaluated. The first natural frequencies of two resonant fixtures are designed as 6,600 Hz (resonator type 1) and 1,100 Hz (resonator type 2), respectively. Two resonant fixtures are made of stainless steel 304. The shock simulation experiment is performed three times for each resonant fixture. Figure 19 shows the measured acceleration SRS at 30 mm, 150 mm, and 350 mm from the shock source. In case of resonator type 1, the resonance response occurs at 3,800 Hz. The resonance response of resonator type 2 occurs at 900 Hz. The knee frequency is lower than the designed frequency, which is mainly due to the influence of the test structure. Note that we can adjust the knee frequency of the shock simulator by using resonant fixtures with different natural frequencies.

4. Conclusion

This paper proposes a compact point-source pyroshock simulator without explosive devices for the pyroshock propagation test. The developed simulator is much more compact than other pyroshock simulators and has repeatability on a shock path from the shock source. For the pyroshock test, the pyroshock measurement instruments were prepared and repeated tests were performed to evaluate the feasibility of the pyroshock propagation test. In order to design the pyroshock simulator in a compact size and applicable on various positions of real structures, the high-pressure air release mechanism consisting of the air tank, the solenoid valve, and the indented diaphragm was built. To increase the repeatability of the simulator, the

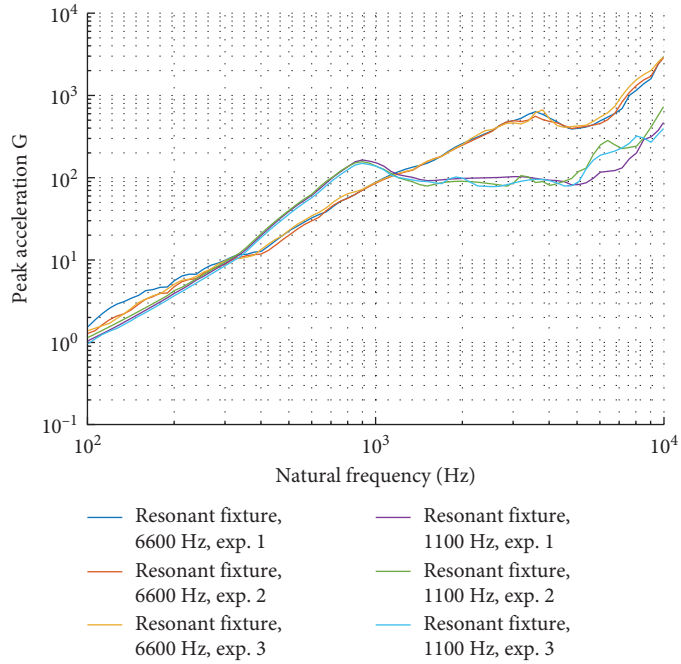

(a)

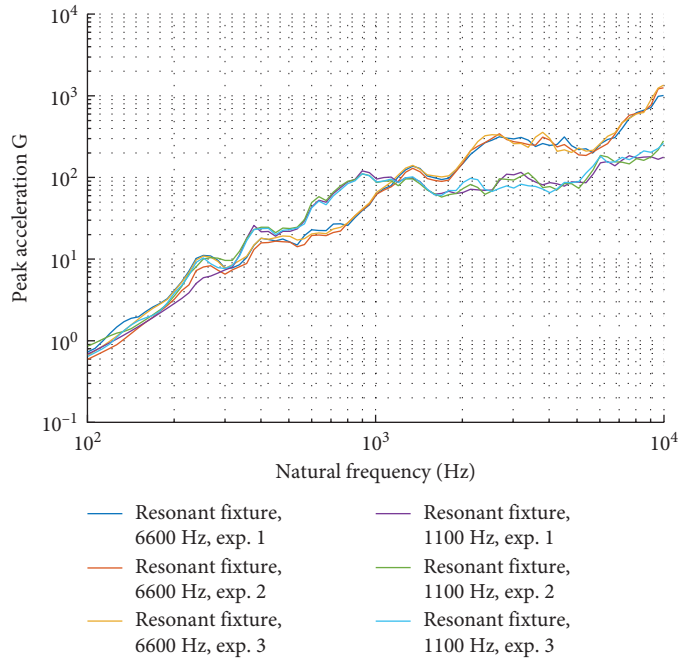

(b)

Figure 19: Continued.

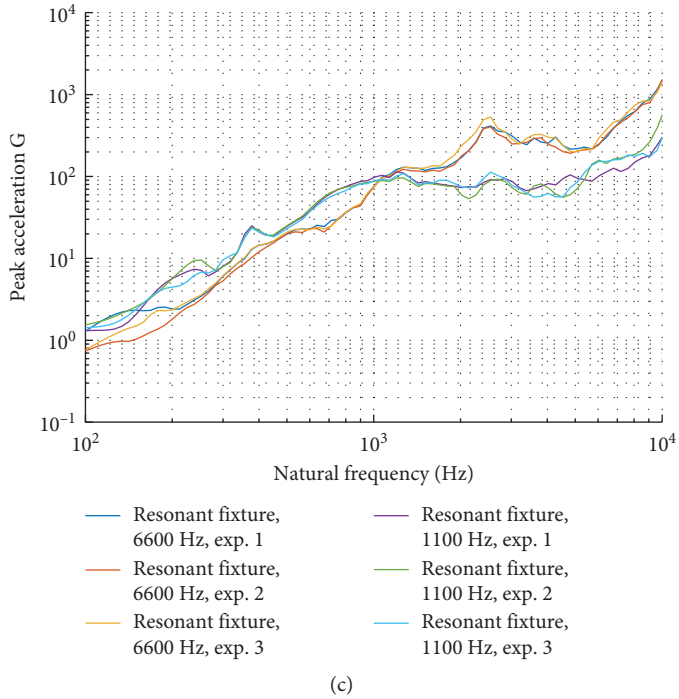

(c)

Figure 19: Acceleration SRS of the pyroshock simulator using resonator 1 and resonator 2 (a) at 30 mm, (b) at 150 mm, and (c) at 350 mm from shock source.

diaphragm was designed to burst in the same shape at a certain pressure by indenting a Y-shape on the center. The effect of the indentation on the diaphragm was analyzed using explicit analysis. To simulate various pyroshock environments, the knee frequency should be adjustable. The knee frequency of the generated pyroshock can be easily changed by using the resonator with different natural frequencies.

Data Availability

Data presented herein are not freely shareable because this research is a classified program of the funding institution.

Conflicts of Interest

The authors declare that there are no conflicts of interest regarding the publication of this paper.

Acknowledgments

This work was supported by the Global Surveillance Research Center (GSRC) program funded by the Defense Acquisition Program Administration (DAPA) and Agency for Defense Development (ADD).

References

[1] C. J. Moening, "Pyrotechnic shock flight failures," in *Proceedings of 31st Annual Technical Meeting of the Institute of Environmental Sciences*, Las Vegas, NV, USA, January 1985.

[2] European Cooperation for Space Standardization, *Mechanical Shock Design and Verification Handbook, ECSS-E-HB-32-25A*, European Cooperation for Space Standardization, Noordwijk, Netherlands, 2015.

[3] H.-K. Jeong, J.-H. Han, S.-H. Youn et al., "Frequency tunable vibration and shock isolator using shape memory alloy wire actuator," *Journal of Intelligent Material Systems and Structures*, vol. 25, no. 7, pp. 908–919, 2014.

[4] W. J. Kacena, M. B. McGrath, and W. P. Rader, *Aerospace Systems Pyrotechnics Shock Data (Ground Test and Flight)*, NASA, Washington, DC, USA, NASA-CR-116437, 1970.

[5] W. J. Kacena, M. B. McGrath, and W. P. Rader, *Aerospace Systems Pyrotechnics Shock Data (Ground Test And Flight)*, NASA, Washington, DC, USA, NASA-CR-116437, 1970.

[6] NASA, *Pyroshock Test Criteria*, NASA, Washington, DC, USA, NASA-STD-7003A, 2011.

[7] Department of Defense, *Environmental Engineering Considerations and Laboratory Tests, Method 517.1, MIL-STD-810G*, Department of Defense, Arlington, VA, USA, 2008.

[8] S. Barret, W. P. Rader, and K. R. Payne, *Viking Dynamics Experience with Application to Future Payload Design*, NASA Langley Research Center, Hampton, VA, USA, NASA-CR-3014, 1978.

[9] S. Barrett and W. J. Kacena, "Method of attenuating pyrotechnic shock," in *Proceedings of 42nd Symposium on Shock and Vibration*, Key West, FL, USA, November 1971.

[10] General Environmental Verification Standard (GEVS) for GSFC Flight Programs and Projects, GSFC-STD-7000A, 2013.

[11] D. Dilhan, V. Cipolla, H. Grzeskowiak et al., "Pyroshock generation," in *Proceedings of the European Conference on Spacecraft Structures, Materials and Mechanical Testing*, Noordwijk, Netherlands, May 2005.

[12] D. Dilhan, A. Piquereau, L. Bonnes, and J. Van de Veire, "Definition and manufacturing of the pyroshock bench," in *Proceedings of the 7th ESA/CNES International Workshop on*

Space Pyrotechnics, Noordwijk, Netherlands, November 2008.

[13] N. T. Davie and V. I. Bateman, "Pyroshock testing, chapter 26, part 2," in *Harris' Shock and Vibration Handbook*, Sandia National Laboratories, Albuquerque, NM, USA, 1996.

[14] N. T. Davie and V. I. Bateman, *Pyroshock Simulation for Satellite Components Using a Tunable Resonant Fixture-Phase 1, SAND 92-2135*, 1992.

[15] N. T. Davie, "Simulation of pyroshock environments using a tunable resonant fixture," S-76, 887 Patent application, SN: 08/128, 963, 1993.

[16] T. Newell and N. James, "Mechanical impulse pyro shock (MIPS) simulation," in *Proceedings of Workshop on Accelerated Stress Testing*, IEEE, Boston, MA, USA, October 1999.

[17] E. Filippi, F. Cambier, and C. Conti, "Development of the Alcatel ETCA pyroshock test facility," in *Proceedings of the European Conference*, Braunschweig, Germany, November 1998.

[18] E. Filippi, H. Attouoman, and C. Conti, "Pyroshock simulation using the Alcatel ETCA test facility," in *Proceedings of First European Conference on Launch Vehicle Vibrations*, CNES, Toulouse, France, December 1999.

[19] G. Schweickert, "The Dornier shock table-a new facility for shock testing of components," in *Proceedings of the Third International Symposium on Environmental Testing for Space Programs*, Noordwijk, Netherlands, June 1997.

[20] M. Jonsson, "*Development of a shock test facility for qualification of space equipment*," M.S. thesis, Division Dynamics, Chalmers University of Technology, Göteborg, Sweden, 2012.

[21] V. I. Bateman and F. A. Brown, "Evaluation of shock mitigating materials in a V-band pyroshock environment simulated with a resonant fixture," *Journal of the IES*, vol. 37, no. 5, pp. 40–45, 1994.

[22] J.-W. Jeong, J.-H. Lim, K.-W. Kim et al., "Development of a point pyroshock source simulator," *Shock and Vibration*, vol. 2017, Article ID 6834601, 16 pages, 2017.

[23] I. M. Hutchings and R. E. Winter, "A simple small-bore laboratory gas gun," *Journal of Physics E: Scientific Instruments*, vol. 8, no. 2, pp. 84–86, 1975.

[24] G. R. Fowles, G. E. Duvall, J. Asay et al., "Gas gun for impact studies," *Review of Scientific Instruments*, vol. 41, no. 7, pp. 984–996, 1970.

[25] Z. J. Rohrbach, T. R. Buresh, and M. J. Madsen, "Modelling the exit velocity of a compressed air cannon," *American Journal of Physics*, vol. 80, no. 1, pp. 24–26, 2012.

[26] ANSYS, Inc., *Introduction to ANSYS Explicit STR, V15.0*, ANSYS, Inc., Canonsburg, PA, USA, 2014.

[27] A. R. Kolaini, R. Nayeri, and D. L. Kerm, *Pyroshock Simulation Systems: Are We Correctly Qualifying Flight Hardware for Pyroshock Environments?*, Pasadena, CA, USA, 2009.

[28] T. Irvine, *An Introduction to the Shock Response Spectrum, Revision S*, 2012.